HHS Public Access

Author manuscript

Mater Today (Kidlington). Author manuscript; available in PMC 2017 April 01.

Published in final edited form as:

Mater Today (Kidlington). 2016 April ; 19(3): 157–168. doi:10.1016/j.mattod.2015.08.022.

Magnetite nanoparticles for cancer diagnosis, treatment, and treatment monitoring: recent advances

Richard A. Revia and **Miqin Zhang***

Department of Materials Science and Engineering, University of Washington, Seattle, WA 98195, USA

Abstract

The development of nanoparticles (NPs) for use in all facets of oncological disease detection and therapy has shown great progress over the past two decades. NPs have been tailored for use as contrast enhancement agents for imaging, drug delivery vehicles, and most recently as a therapeutic component in initiating tumor cell death in magnetic and photonic ablation therapies. Of the many possible core constituents of NPs, such as gold, silver, carbon nanotubes, fullerenes, manganese oxide, lipids, micelles, etc., iron oxide (or magnetite) based NPs have been extensively investigated due to their excellent superparamagnetic, biocompatible, and biodegradable properties. This review addresses recent applications of magnetite NPs in diagnosis, treatment, and treatment monitoring of cancer. Finally, some views will be discussed concerning the toxicity and clinical translation of iron oxide NPs and the future outlook of NP development to facilitate multiple therapies in a single formulation for cancer theranostics.

Introduction

The development of nanoscale technologies has been widely touted as a revolutionary paradigm shift for detection and remediation of cancer. Indeed, the surge in research efforts exploring the design and synthesis of nanoparticle (NP) systems has seen the creation of many material formulations exhibiting promising therapeutic and diagnostic (theranostic) effects towards the treatment of various cancer types in a single nanodrug[1–3]. NP configurations include those with fundamental cores of organic molecules (e.g. dendrimers, DNA, lipids, viruses, and micelles), inorganic molecules (e.g. iron oxide, gold, quantum dots, carbon nanotubes, and fullerenes), or a hybrid of two or more of these components[4,5]. Each base structure has associated advantages and disadvantages that depend on the application under consideration. Furthermore, these formulations have properties that are tunable to some degree, such as size, surface charge, and hydrophobicity, allowing them to be optimized for a desired function.

Iron oxide NPs with nanocrystalline magnetite (Fe_3O_4) cores have great potential for use in oncological medicine due to their biocompatibility[6], biodegradability[7], facile synthesis[8], and ease with which they may be tuned and functionalized for specific applications. Additionally, spherical magnetite NPs with diameters less than approximately 20 nm will

*Corresponding Author: Miqin Zhang (mzhang@uw.edu).

exhibit superparamagnetic behavior, a property that is exploited to enhance contrast in magnetic resonance imaging (MRI)[9–11]. Typically, superparamagnetic iron oxide nanoparticle (SPION) conjugates are comprised of a magnetite core providing inherent contrast for MRI and a biocompatible coating that provides ample functional groups for conjugation of additional tumor targeting and therapeutic moieties. As some formulations of magnetite-based NPs have already gained approval for use in humans as iron deficiency therapeutics and as MRI contrast agents by the Food and Drug Administration (FDA) (e.g. Feraheme®, Feridex I.V.®, and Gastromark®), extension of these NP configurations for uses beyond MRI contrast enhancers such as cancer therapeutics via drug delivery, biotherapeutic transport, magnetic hyperthermia, photothermal ablation, and photodynamic therapy (PDT) may be fast-tracked as compared to NP formulations lacking widespread acceptance of nontoxicity (e.g. other metal-core NPs)[11]. This idea highlights the considerable capacity iron oxide NPs have for use in highly personalized medicine; as researchers develop a library of synthesis protocols and discrete nanoscale modules with specific roles for cancer theranostics, individualized NP formulations exhibiting a full-suite of treatment and diagnostic capabilities may be created in an efficient and effective manner. An exemplary NP incorporating a multitude of diagnostic and therapeutic features is depicted in Fig. 1.

There are a few reviews focusing on the development and applications of magnetite NPs[12–16]; this article aims to provide an update of the new findings in the merging field since 2013. This review discusses recent advances in employing iron oxide-core NPs for diagnosis and monitoring of cancer through imaging modalities, the treatment of tumors via transportation of chemotherapeutic and biotherapeutic agents (i.e. drugs, nucleic acids, and proteins), magnetic hyperthermia and photothermal therapies, as well as PDT. Finally, overview of the new concept of NanoEL and nanotoxicity of metal-oxide NPs and some remarks regarding the translation of nanotherapeutics into a clinical setting are provided.

SPIONs in cancer diagnosis and treatment monitoring

Imaging tumorous tissue is of paramount importance in the diagnosis and treatment monitoring of cancer[17,18]. Clear depictions of tumor boundaries allow for accurate judgments of tumor distribution and its response to surgical removal and adjuvant therapies. Many imaging modalities are employed for early detection and interrogation of cancer, including X-ray, ultrasound, MRI, computed tomography (CT), and positron-emission tomography (PET)[17]. Iron oxide NPs have been extensively researched for their use in augmenting contrast for MRI[19]; recently, hybrid NP formulations with superparamagnetic iron oxide cores modified with exterior coatings and functional probes have been devised for their ability to enhance contrast in alternative imaging techniques in addition to MRI.

Contrast enhancing NPs that can selectively accumulate at tumor sites help to provide precise information regarding tumor extent. The method of NP accumulation at tumor sites is typically categorized into two separate classes: passive and active targeting. Passive targeting relies on the enhanced permeability and retention (EPR) effect[20]. A hallmark of cancerous tissue is the formation of a perforated vasculature and maladroit intratumoral lymphatic drainage. NPs less than approximately 100 nm can pass through such leaky

vessels into the tumor microenvironment and remain for an amount of time that is significantly longer than the blood clearance of the NPs; this is the EPR effect[21]. Passive targeting is limited however because not all tumors exhibit the EPR effect and the degree of permeability of the tumor vasculature is unlikely to be homogenous across the whole site[22]. Attempts at overcoming these limitations are made with active targeting. Active targeting is achieved by modifying an NP through the attachment of a targeting ligand to the NP surface. Ligands that recognize biological structures unique to or overexpressed in cancer cells can then preferentially accumulate at tumor sites. A third mode of targeting unique to magnetic NPs such as SPIONs is the use of an external magnetic field to draw the NPs to the site of action[23]. All three of these targeting mechanisms are presently being employed in the development of SPIONs as imaging agents. The vast majority of SPION formulations are in preclinical development, although there are a number of studies using the iron oxide NP ferumoxytol as an MRI contrast agent currently undergoing clinical trials[24–27].

Recently, it was shown that iron oxide NPs as well as other NP formulations, induce gaps tens of microns in size between endothelial cells (i.e., cells that form the interior walls of blood vessels)[28,29]. The mechanism by which NPs cause such openings was dubbed nanoparticle-induced endothelial leakiness (NanoEL)[30,31]. Prior to the discovery of NanoEL, the routes for NPs to escape the endothelium were thought to be confined to typical transcellular endocytosis and diffusional transport through cell membranes via cell-cell junctions; however, these methods of NP transport through the endothelium alone are not sufficient to explain the speed with which NPs have been shown to enter certain highly vascularized organs like kidneys, liver, and spleen[30]. NanoEL occurs much more rapidly than either endocytosis or diffusion through cell-cell junctions. The phenomenon of NanoEL is described by the intracellular binding of NPs to VE-cadherin; following this pairing, phosphorylation of VE-cadherin is triggered which in turn results in a rearrangement of the endothelial cell cytoskeleton[32]. This insight into the interaction of NPs with biological environments is of paramount importance as it may provide an explanation for the physical mechanism by which off-target accumulation of NPs at sites other than tumors happens. Further exploration into how specific NP characteristics like size and surface charge alter the behavior of the NanoEL effect may help nanotechnologists to mitigate off-target NP accumulation and even exploit induced endothelial leakiness for therapeutic effects.

Magnetic resonance imaging

MRI is an immensely important tool in medicine offering detailed spatial resolution and soft tissue contrast without the use of ionizing radiation or potentially harmful radiotracers[33,34]. In MRI, a large external magnetic field is applied to a sample of interest resulting in an alignment of the magnetic moments of the protons within the sample. When SPIONs are present in such a system, their magnetic moments couple with the magnetic moments of nearby protons causing spin dephasing and a shortening of the relaxation times of protons in the vicinity[35]. Typically, SPIONs are thus used to provide negative (hypointense) contrast by darkening T_2- and T_2*-weighted images in voxels containing SPIONs.

Much attention has been devoted to optimizing SPION formulations for their use in enhancing MRI contrast; parameters of SPIONs such as surface coating[36], shape[37], and

composition[38] are all important factors in determining the magnetic and biological behavior of SPIONs. The nanoscale size of iron oxide NPs results in a high surface area-to-volume ratio, which in turn results in large surface energies. Therefore, passivation of the iron oxide cores of SPIONs is needed to achieve favorable *in vivo* behavior. Without an inert coating, iron oxide NPs are subject to opsonization and rapid clearance from the blood by the reticuloendothelial system (RES). SPIONs developed for MRI contrast have been coated with a variety of passivating materials such as polyethylene glycol (PEG)[39], chitosan[40], dextran[41], and other polymers[42]. The magnetic properties of SPIONs are altered with the addition of surface coatings, and as such, care must be taken to ensure that a proper balance between desirable pharmacokinetics and magnetic responses is met when adding passivation layers. The size of iron oxide cores is another parameter that affects the magnetic properties of NPs[43]. Considering SPIONs with diameters between 4 and 20 nm, as the particle size increases, so does the negative contrast provided in T_2-weighted images[37,44]. This phenomenon provides some degree of tunability in the T_2 contrast effect of SPIONs.

While SPIONs have historically been used primarily for negative contrast enhancement by darkening T_2-weighted images, they may also be customized to provide positive contrast enhancement in T_1-weighted scans[45,46]. T_1 contrast is most commonly provided by potentially toxic gadolinium (Gd) chelates[47]. SPIONs offer an advantage over Gd-based agents due to both their non-toxicity and superiority in providing T_1 contrast. For instance, a SPION formulation has been developed exhibiting a two-fold improvement of T_1 contrast enhancement as compared to a commercial Gd-based clinical standard[45].

To increase the efficacy of SPIONs as MRI contrast agents for monitoring cancer, targeting of solid tumors is enhanced in SPIONs by exploiting tumor biomarkers. SPIONs recently developed to provide contrast in T_2-weighted MRI were conjugated with a deimmunized mouse monoclonal antibody (muJ591) to target a prostate biomarker[48]. These iron oxide-core NPs were able to specifically target prostate cancer cells showing their potential for use as a diagnostic imaging agent.

Multimodal imaging

Even though SPIONs were specifically developed for use as MRI contrast agents, recent efforts have been made to incorporate additional functions to provide complementary imaging modalities. Multimodal imaging enhancement agents allow investigators and physicians to use NPs on a number of imaging platforms including magnetic resonance[49], optical[50], CT[41], PET[51], photoacoustic[52], and other imaging systems[53]. Each of the imaging methods has benefits and drawbacks. MRI has exceptional spatial resolution but lacks sensitivity. Optical imaging is relatively inexpensive and very sensitive but cannot penetrate deep into all tissues due to the scattering of light. Similarly, CT is characterized by high spatial resolution and low sensitivity whereas PET is highly sensitive yet provides no structural information. Thus, combinations of these imaging modalities provide the anatomical resolution and molecular sensitivity needed for accurate diagnoses of cancers, and with one material serving as the contrast agent for multiple imaging modalities, the accuracy and consistency of diagnosis can be significantly improved.

SPIONs with complementary optical contrast enhancing capabilities via fluorescent probes are considered promising since the combined preoperative anatomical information from MRI and intraoperative molecular detail provided by fluorescence imaging could give surgeons a precise delineation of cancer tissue[52,54]. In fluorescence imaging, an external light source is applied to a sample, fluorophores absorb energy from this source and almost immediately emit detectable photons at a longer wavelength and lower energy than the source[55]. An important consideration in the design of a fluorescence imaging system is the desired penetration depth. A common choice for achieving larger penetration depths in tissue is to use a near-infrared (NIR) source and fluorophores that emit NIR light. One such dye that has been conjugated onto SPIONs to produce a dual-mode imaging contrast agent is Cy5.5[56,57]. These imaging probes have shown an excellent ability to provide both MRI and fluorescence contrast in murine tumor models.

NPs consisting of bismuth-iron oxide composite cores were synthesized to provide a dual-mode imaging contrast agent[41]. Iron oxide provided MRI contrast whereas the heavy metal bismuth acted as the X-ray attenuating agent required for CT. The inclusion of bismuth in the iron oxide core did result in a decrease in the MRI contrast ability of the NPs, but *in vivo* MRI and CT scans nonetheless showed excellent contrast from the NPs in both imaging. In Fig. 2a, the CT contrast efficacy of these NPs is evident from the clear depiction of soft tissue just five minutes after injection compared to the complete absence of such organs prior to the introduction of NP into the body. Further proof of the CT contrast enhancement of these NPs is depicted in the CT images of a mouse thorax in Fig. 2b, the CT images of a mouse groin in Fig. 2c, and the CT signal attenuation quantified in various organs over time in Fig. 2d. The MRI contrast enhancing capability of these NPs is depicted for a mouse liver in Fig. 2e and quantified in Fig. 2f. PET imaging offers extremely high sensitivity and limitless tissue penetration[58]. The PET isotope ^{18}F was introduced to iron oxide core NPs producing a trimodal contrast agent capable of detection through PET, fluorescence imaging, and MRI[59]. While many SPION formulations have been produced to create contrast agents with multimodal capabilities, there is still a lack of integrated imaging systems hampering their widespread use.

Monitoring cancer treatment with SPIONs

At present, cancer treatment efficacy is typically evaluated through *ex vivo* assessments of biopsies or comparison of structural images of anatomic tissue pre- and post-therapy[60]. The time between therapy commencement and the initial treatment appraisal can be weeks or even months. Such a lag in effective treatment monitoring inhibits optimal therapy by delaying opportunities to adjust treatment methods such as altering chemotherapeutic dosages. SPIONs have the potential to provide real-time treatment monitoring of therapeutic drug delivery as well as tissue response, thereby expediting updates to treatment regimens and improving a patient's quality of life.

One way in which SPIONs may be employed for treatment monitoring is by providing accurate knowledge about drug administration and distribution. For example, SPIONs were used to label murine dendritic cells in order to track their migration *in vivo* with non-invasive MRI[61]. Dendritic cells administered to cancer patients have been shown to induce

increased anti-tumor immune responses by stimulating effector T cells. SPION-labeled dendritic cells showed potential for clinical use in assessing the therapeutic efficacy of dendritic cells by providing a visualization of their localization, thereby informing the relative effective dosage that was received and that the appropriate delivery site was accessed. Other studies have monitored the biodistribution and pharmacokinetic behavior of SPIONs *in vivo* using MRI as the NPs move throughout various organ systems[62–64]. This technique shows the non-invasive tracking capability of magnetite NPs as drugs move to the desired target.

Another method of using SPIONs to monitor drug delivery is by detecting changes in the T_1 and T_2 relaxivity values of iron oxide NPs upon transformation from a drug-loaded to a drug-released state[65]. The drugs Flutax1 (a Taxol derivative), Doxorubicin, and DiR were loaded onto iron oxide NPs and subsequently coated in a pH-sensitive polymeric coating (i.e. a coating that degrades when exposed to acidic environments)[66]. Figures 3a and 3b show that, when loaded onto NPs, all three drugs increase the T_1 and T_2 values of the drug delivery vehicle compared to the native iron oxide NPs. Figure 3c illustrates that as the amount of drug, in this case Flutax1, is increasingly loaded onto NPs, both T_1 and T_2 values increase linearly in response. It is proposed that the increase in relaxivity values that accompany drug loading is due to the inhibition of water diffusion in the vicinity of the iron oxide cores of NPs. Since SPIONs affect MRI contrast by magnetically interacting with nearby protons to shorten relaxation times, drugs loaded onto NPs may hinder water's access to NP cores and thereby nullify their ability to alter the relaxation times of protons. Figure 3d shows that Doxorubicin loaded NPs released the drug when exposed to pH environments of 6.8 or less, and drug release consequently reduced the T_1 and T_2 values of the NPs. This demonstrates how MRI may be used to monitor cargo release from iron oxide NPs.

Therapeutic SPIONs for cancer treatment

This section discusses and provides examples of the use of SPIONs in chemotherapy, gene and protein therapy, magnetic hyperthermia, photothermal ablation, and PDT. Most of the SPION formulations developed for therapeutic purposes are still in the preclinical phase of development and are tested in small rodent models. In developing and implementing any drug for use in humans and animals it is of utmost importance to consider the levels at which the therapeutic agents begin to exhibit toxic effects. In addition to the therapeutic uses of SPIONs, this section also includes the discussion of the potential mechanisms of toxicity exhibited by iron oxide NPs.

Chemotherapeutics

The goal of chemotherapy is to impede the growth of tumor cells through the action of chemicals that inhibit cell function. Drugs have been developed to attack cell function in a number of ways, including the disruption of DNA replication and repair, interfering with protein expression, and other mechanisms of stopping or inhibiting cell division. However, the efficacy of chemical drugs acting alone is limited due to their lack of selectivity in targeting cancer cells, pharmacological limitations, and their toxicity to healthy tissues[67,68].

Encapsulating or attaching molecular drugs to NPs helps selectively deliver chemotherapeutics to target sites, allows for increased dosage, minimizes off-target toxicity, protects drugs from degradation, and enhances biocompatibility[69]. Several cancer chemotherapeutic drugs have been combined with SPIONs including temozolomide (TMZ)[70], doxorubicin[71], paclitaxel[72], and 5-fluorouracil[73].

The DNA alkylating agent TMZ is the current standard-of-care chemotherapeutic in the treatment of glioblastoma (GBM)[74]. Iron oxide NPs were loaded with TMZ by covalently linking TMZ to a chitosan coating layer[70]. These NPs were further functionalized with the addition of chlorotoxin (CTX), a tumor-targeting peptide. Results showed that CTX and TMZ-conjugated NPs had much greater stability compared with that of native TMZ and were able to specifically target GBM cells. Furthermore, CTX and TMZ-conjugated NPs exhibited a 2 to 6-fold increase in uptake by GBM cells compared with nontargeted NPs. Doxorubicin loaded SPIONs have been synthesized and show inhibited growth of xenograft breast tumor in a murine model[71]. MRI was used to monitor the passive accumulation of these SPIONs at the tumor site, thereby exemplifying the efficacy of a contrast enhancing drug delivery vehicle that may be achieved with magnetite NPs.

Biotherapeutics

Biotherapeutic therapy is similar to chemotherapy except that instead of delivering small molecular drugs, biological agents such as DNA, small interfering RNA (siRNA), proteins, and peptides are delivered to tumor sites to induce cell death. In cancer, damaged DNA results in atypical protein expression causing deleterious effects. Cancer may be treated with DNA delivery by replacing the defective genes within cancer cells. Alternatively, cancer therapy via siRNA works by suppressing the protein expression of damaged genes. Protein and peptide therapy, on the other hand, operates by attacking specific cell mechanisms such as disrupting cell adhesion, interfering with angiogenesis, and/or blocking other cellular functions that could lead to apoptosis. In the past, delivery of biotherapeutics has shown limited success due to the immunogenicity caused by the delivery vectors[75]. Inclusion of biotherapeutics in NP delivery systems has promise as biocompatible polymer-coated NPs provide protection against inhibitive immune responses and targeted delivery of these therapeutic agents.

Typically, for gene therapy, NPs are coated with a cationic polymer that encapsulates or binds DNA or siRNA as the positive charge of this layer allows for favorable electrostatic interactions with negatively charged nucleic acids[76]. Other design considerations for DNA delivery include the requirement that NPs need access to the cell nucleus for the successful transfection of genetic material. This is usually accomplished by conjugating peptides that facilitate nuclear localization to the surface of NPs.

As DNA and siRNA drug delivery vehicles must provide protection for the loaded drug from degradation during transportation followed by drug release upon entering the cell, so-called intelligent NPs have been developed that utilize coatings that break down when exposed to an environmental factor that is specific to a particular intracellular space. For instance, iron oxide NPs were coated in a disulfide-containing polyethylimine (PEI) exterior to create redox-sensitive gene delivery vehicles[77]. PEI is a cationic polymer that can bind nucleic

acids through electrostatic interactions. Disulfide-crosslinking of PEI creates a bioreducible coating layer since the disulfide bond is chemically stable in extracellular locations, but intracellularly, the disulfide bond is cleaved due to the presence of glutathione[78].

Recently, an iron oxide-core NP coated with a polymer shell consisting of chitosan, PEI, and PEG was developed[79]. Chitosan was used to provide a stabilizing biocompatible and biodegradable surface coating with active sites for the binding of PEI and PEG. PEI electrostatically binds nucleic acids and was used to load siRNA. Results display successful intracellular delivery of siRNA to medulloblastoma and ependymoma cancer cells and the consequent suppression of a radiation resistant DNA repair protein. The siRNA-mediated suppression of this protein led to reduced tumor cell resistance to γ-rays.

Induced magnetic hyperthermia

The innate magnetic properties of SPIONs may be harnessed to induce localized hyperthermia by applying an external magnetic field making SPIONs therapeutic without the addition of functional moieties (Fig. 4a). Sustained temperatures above 42°C alters many of the structural and functional proteins within cells causing necrosis[80,81]. Applying an external magnetic field operating at a specific frequency and power based on the SPION formulation causes the magnetic NPs to heat by hysteresis loss, Néel relaxation, and induced eddy currents[82].

Recently, PEG-coated magnetite NPs were able to impede tumor growth through magnetic hyperthermia when intratumorally injected into epidermoid carcinoma xenograft implanted mice (Fig. 5)[83]. Figure 5a is composed of thermographic infrared photographs taken at different timepoints during magnetic hyperthermia and shows increased temperatures around a tumor site that was injected with NPs. Figure 5b shows quantitative temperature profiles of various organ systems interrogated during the magnetic hyperthermia therapy; here it is seen that off-site temperature levels retain at normal values whereas the tumor tissue experience elevated temperatures. Results also showed that these NPs exhibited diminished heating capacity upon cell internalization and functioned much better when located in the interstitial extracellular space. Furthermore, the destruction of the extracellular matrix caused by magnetic hyperthermia led to increased drug penetration as evidenced by superior tumor growth impediment when doxorubicin loaded NPs were used with concomitant magnetic hyperthermia compared with treatments of only magnetic hyperthermia or doxorubicin loaded NPs as shown in Fig. 5c.

Another exploitation of the magnetic hyperthermia effect is for use as a drug-releasing trigger. If drugs are encapsulated in a heat-labile coating, then controlled release of drugs may be achieved with magnetite NPs when they heat up due to the application of an external magnetic field. Hydrophilic doxorubicin and iron oxide NPs were encapsulated in a shell of poly(vinyl alcohol) (PVA)[84]. PVA was chosen because of its ability to load hydrophobic paclitaxel. Thus, these NPs contained two potent chemotherapeutics with drastically different characteristics in one NP. Furthermore, when these NPs were subjected to an external 50 kHz magnetic field, the release rate of both drugs increased and then decreased when the field was removed. This shows great potential for SPION use as on-demand drug

release vehicles as it is relatively simple to control heating with magnetite NPs by adjusting the intensity and duration of the applied magnetic field[85].

Photothermal ablation

Photothermal therapy utilizes a visible or NIR laser light source to activate thermal heating of NPs through photon absorption (Fig. 4b)[86]. Typically, gold-core or gold-coated NPs are employed in photothermal therapy due to their ability to absorb NIR wavelengths, a region of the electromagnetic spectrum that offers optimal tissue penetration[87].

NPs with iron oxide cores and gold shells have been developed for use in targeted photothermal destruction of colorectal cancer cells[88]. Gold and iron oxide hybrid NPs were functionalized with a single chain antibody for active targeting of the A33 antigen, which is overexpressed in colorectal cancer cells. Results showed that cells expressing the A33 antigen internalized NPs five times faster than cells not expressing the antigen. Furthermore, after six minutes of exposure to an 800 nm laser radiation at 5.1 W cm^{-2}, 53% of A33-expressing cells died while less than 5% of A33 non-expressing cells died. This shows excellent selectivity for cancer cell death.

In another application of gold-coated magnetite NPs for targeted photothermal ablation of cancer cells, further exhibition of the bimodal imaging capabilities of such particles for use as MRI and optical contrast agents was shown[89]. Again, highly selective cancer cell death was achieved by functionalizing the NPs with epidermal growth factor receptor, a prevalent biomarker for epithelial cancer. SPION development continues for use in photothermal therapy and as imaging agents due to their inherent MRI contrast[90,91].

Photodynamic therapy

PDT has been in development as a cancer therapy for over 50 years; it involves the use of photosensitizing agents localized in tumor tissues and their subsequent activation by an external light source of a specific wavelength (Fig. 4c)[92]. Upon activation, photosensitizers generate singlet oxygen ($^1O_2$) which is acutely cytotoxic and causes irreversible free radical damage to tissues within a distance of approximately 20 nm[93]. The efficacy of PDT is limited by the short distances and lifetimes over which photosensitizing agents operate[94]. To enhance their impact, increased targeting of photosensitizing agents has been achieved through their attachment to iron oxide NPs as functional ligands. MRI contrast enhancing iron oxide NPs have been conjugated with a fluorescent photosensitizing agent pheophorbide-A[94]. The pheophorbide-A-conjugated NPs were activated with a 670 nm laser source to generate cytotoxic $^1O_2$ species and showed further promising bimodal fluorescence/MRI contrast capabilities. Photosensitizing agent chlorin e6 (Ce6) was shown to have greatly accelerated cellular uptake when conjugated to PEGylated iron oxide NPs as compared to free Ce6[95]. These Ce6-conjugated NPs were magnetically drawn to tumor sites as shown schematically in Fig. 6a. Figures 6c and 6d show *in vivo* fluorescence and MR images of a tumor-bearing mouse injected with Ce6-conjuated NPs respectively. Figures 6d and 6e depict quantitative measurements of the fluorescence and MRI signal intensities for two different tumor regions: one that was not exposed to an external magnetic field to draw in NPs and another that did undergo magnetic field targeting. *In vivo* photodynamic

treatment with these particles has been shown to significantly delay tumor growth in a mouse model as can be seen from Figures 6f and 6g. In contrast to functionalizing iron oxide NPs with photosensitizing agents, photosensitive fullerenes have been decorated with magnetite NPs to add MRI contrast capabilities to create a theranostic system[96].

Many applications of SPIONs have been discussed thus far, and each NP formulation mentioned is unique in surface coating, size, and the specific application it was designed for. To provide an aid in summarizing some of the literature discussed herein, Table 1 arranges noteworthy information about some current research so that a quick identification of the wide variety of applications that exist for SPIONs in cancer diagnosis and treatment may be made.

SPION Toxicity

While a number of iron oxide NP formulations have been approved by the FDA, this acceptance does not mean that SPIONs may be administered to the body with impunity. Many studies concerning SPION toxicity have been carried out with both uncoated SPIONs and iron oxide NPs passivated with a variety of different surface layers[97]. The general consensus seems to indicate that iron oxide NPs exhibit very little or no cytotoxic activity when administered concentrations remain below a 100 μg/mL threshold[98]. However, it has also been shown in both *in vitro* and *in vivo* studies that SPIONs, both coated and uncoated, can harm cell behavior via numerous mechanisms including the disruption of cytoskeletons, inducement of oxidative stress, generation of free radicals, impairment of mitochondrial function, damage of DNA, and altering of cell signaling pathways among others[97,99]. Many toxicities of these modified SPIONs may not be caused by the SPIONs but the coatings that cause nanoparticles agglomerate and unstable in biological media and serum. Note that any aggregated nanoparticles regardless materials will be toxic to cells and tissues.

Properties of SPIONs that are typically tuned based on the given application, such as particle size and surface coating, also play a role in determining the toxicity of the NP formulation. In one study employing PVA-coated iron oxide NPs, it was found that both the shape of the NP (e.g., sphere, rode, and beads) as well as the mass ratio of polymer coating to iron had a direct influence on toxicity[100]. Given that even subtle changes in NP formulation can lead to significant changes in cytotoxicity behavior, it seems that the toxicity of each unique NP configuration must be evaluated prior to animal studies.

SPIONs in translational research

A large number of NP contrast agents and cancer therapeutics have shown excellent results when used in murine and other small animal models. However, the translation of these NP formulations to use in the medical clinic fails at a very high rate as can be corroborated with the relative dearth of NPs employed for use in humans[101,102]. Specifically for iron oxide NPs, only a handful of formulations have been approved by the FDA, and even the most recent magnetite-based NP to be approved, Feraheme®, does not have an intended use as an MRI contrast agent or cancer therapeutic[42]. Other iron oxide NP formulations, although approved by the FDA, have stopped being marketed by their manufacturers (e.g. Feridex I.V.® and Gastromark®). Currently, no functionalized SPIONs are used in humans.

Clinical studies for application of hyperthermia therapy using SPIONs in humans were initiated in 2007 on prostate cancer and glioblastoma patients[103,104]. The results demonstrated that interstitial heating using iron oxide NPs was feasible and well tolerated in patients with locally recurrent prostate cancer. Recent trials in evaluating the feasibility and tolerability of thermotherapy in patients with recurrent glioblastoma multiforme showed that patients treated with hyperthermia had double the median overall survival time compared to the control[105]. More recently, iron oxide NPs were used in hyperthermia therapy to treat metastatic bone tumors, and reduced lesion and visible bone formation were observed[106].

The successful translation of NP into a clinical setting is strongly dependent upon their physicochemical properties, toxicity, drug loading capacity, and functionalization capabilities. The development of clinically translatable NPs should meet some key criteria. NPs should be composed solely of non-toxic materials or materials that biodegrade into components that may be totally cleared by the liver and kidneys. NPs should have biologically inert, hydrophilic, and neutral surface coatings such as PEG to slow the rate of the clearance from the blood and retention in the RES. Degraded components from NPs should have a hydrodynamic size less than 5 nm so they will be excreted in the urine in a short amount of time[107]. NPs should have high drug loading capacity and be able to release drugs in a controlled manner. For clinical use of SPIONs in hyperthermia, SPIONs must be able to have a homogenous distribution and reach uniform therapeutic temperature throughout tumor tissues and induce minimal damage to peritumoral tissues.

Conclusions and outlook

Iron oxide NPs show great promise for use as imaging contrast enhancement and adjuvant therapy agents for cancers that are traditionally treated with a combination of surgical resection, radiation therapy, and chemotherapy. Furthermore, these NPs exhibit great potential for use in monitoring cancer therapies and could provide crucial information to physicians allowing them to adapt treatment strategies to provide optimal care. Magnetite-core NPs have seen widespread development by research teams throughout the world, yet few formulations have been approved for clinical uses. Low drug loading capacity, insufficient tissue selectivity, and a lack of control over the biodistribution of SPIONs are the major issues holding back their clinical translation. Nevertheless, improvements in controlling SPION size, shape, and surface modifications have helped to gain better magnetic behaviors as well as improved tissue targeting, pharmacokinetics, and biodistribution.

Current efforts to develop SPIONs for cancer theranostics have continued unabated. There are quite a few ongoing clinical trials utilizing magnetite-core NPs for the diagnosis of various cancers and hyperthermia therapy. Furthermore, research teams continue to develop and optimize synthesis techniques for functionalization of SPIONs with a wide variety of imaging contrast, chemotherapeutic, and biotherapeutic agents; development of multimodal therapeutic approaches by combining the dual effects of magnetic hyperthermia and chemotherapy as well as using multiple drugs in a single SPION formulation will help to push iron oxide NPs into the forefront of cancer treatment agents.

Translation of SPIONs from the bench side into the clinic requires a total comprehension of the effects that NP parameters (e.g. size, chemical reactivity, formulation, stability, biodegradability) have on the biological responses of the human body. While many NP formulations have shown excellent result in small animal models, far too many fail to reproduce the same level of therapy in large animal models and humans. To increase the success rate of translating NPs into the clinic, efforts should be focused on improving their drug loading capacity, increasing their specificity and affinity to target cancer cells, and gaining proficiency in microenvironment-dependent controlled drug release. Furthermore, better theoretical *in vitro* and animal models will help to predict the optimal NP formulation for humans. As our understanding of NP behavior in biological environments improves, we are optimistic that integrated imaging and multimodal therapy with iron oxide NPs will push forward the clinical use of SPIONs in the near future and dramatically impact the treatment of cancers.

Acknowledgments

We acknowledge the support of NIH Grants R01CA161953. RR acknowledges College of Engineering Dean's Fellowship and ARCS Foundation fellowship at University of Washington.

References

1. Ryu JH, et al. Advanced Drug Delivery Reviews. 2012; 64(13):1447. [PubMed: 22772034]
2. Sanna V, et al. International Journal of Nanomedicine. 2014; 9:467. [PubMed: 24531078]
3. Veiseh O, et al. Advanced Drug Delivery Reviews. 2010; 62(3):284. [PubMed: 19909778]
4. Cheng Y, et al. Advanced Drug Delivery Reviews. 2014; 66(0):42. [PubMed: 24060923]
5. Kievit FM, Zhang M. Advanced Materials. 2011; 23(36):H217. [PubMed: 21842473]
6. Sun C, et al. ACS Nano. 2010; 4(4):2402. [PubMed: 20232826]
7. Weissleder R, et al. American Journal of Roentgenology. 1989; 152(1):167. [PubMed: 2783272]
8. Sun C, et al. Advanced Drug Delivery Reviews. 2008; 60(11):1252. [PubMed: 18558452]
9. Stephen ZR, et al. Materials Today. 2011; 14(7–8):330. [PubMed: 22389583]
10. Gossuin Y, et al. Wiley Interdisciplinary Reviews: Nanomedicine and Nanobiotechnology. 2009; 1(3):299. [PubMed: 20049798]
11. Krishnan KM. IEEE transactions on magnetics. 2010; 46(7):36.
12. Rosen JE, et al. Nanomedicine: Nanotechnology, Biology and Medicine. 2012; 8(3):275.
13. McCarthy JR, Weissleder R. Advanced Drug Delivery Reviews. 2008; 60(11):1241. [PubMed: 18508157]
14. Yen SK, et al. Theranostics. 2013; 3(12):986. [PubMed: 24396508]
15. Kievit FM, Zhang M. Advanced materials. 2011; 23(36):H217. [PubMed: 21842473]
16. Kievit FM, Zhang M. Accounts of chemical research. 2011; 44(10):853. [PubMed: 21528865]
17. Song SE, et al. Cancer Imaging. 2015; 15(1)
18. Thurber GM, et al. J. Surg. Oncol. 2010; 102(7):758. [PubMed: 20872807]
19. Hao R, et al. Advanced Materials. 2010; 22(25):2729. [PubMed: 20473985]
20. Maeda H, et al. J. Control. Release. 2000; 65(1–2):271. [PubMed: 10699287]
21. Chiarelli PA, et al. Surg. Neurol. Int. 2015; 6(Suppl 1):S45. [PubMed: 25722933]
22. Peer D, et al. Nature Nanotechnology. 2007; 2(12):751.
23. Subbiahdoss G, et al. Acta Biomaterialia. 2012; 8(6):2047. [PubMed: 22406508]
24. ClinicalTrials.gov [Internet]. Bethesda, MD: National Library of Medicine, US; 2015. M.D. Anderson Cancer Center, Ferumoxytol - Iron Oxide Nanoparticle Magnetic Resonance Dynamic

Contrast Enhanced MRI. 2000 Available from: http://clinicaltrials.gov/show/NCT01895829 NLM Identifier: NCT01895829 [cited 2015 March 29]

25. ClinicalTrials.gov [Internet]. Bethesda, MD: National Library of Medicine, US; 2013. Massachusetts General Hospital, Pre-Operative Nodal Staging of Thyroid Cancer Using Ultra-Small Superparamagnetic Iron Oxide Magnetic Resonance Imaging (USPIO MRI): Preliminary Study. 2000 Available from: http://clinicaltrials.gov/show/NCT01927887 NLM Identifier: NCT01927887 [cited 2015 March 29]
26. ClinicalTrials.gov [Internet]. Bethesda, MD: National Library of Medicine, US; 2015. M.D. Anderson Cancer Center, UPSIO Magnetic Resonance Imaging (MRI). 2000 Available from: http://clinicaltrials.gov/show/NCT01815333 NLM Identifier: NCT01815333 [cited 2015 March 29]
27. OHSU Knight Cancer Institute. ClinicalTrials.gov [Internet]. Bethesda, MD: National Library of Medicine, US; 2014. Imaging Vascular Properties of Pediatric Brain Tumors Using Ferumoxytol and Gadolinium in a Single Imaging Session. 2000 Available from: http://clinicaltrials.gov/show/NCT00978562 NLM Identifier: NCT00978562 [cited 2015 March 29]
28. Setyawati MI, et al. Nat Commun. 2013; 4:1673. [PubMed: 23575677]
29. Astanina K, et al. Acta Biomaterialia. 2014; 10(11):4896. [PubMed: 25123083]
30. Setyawati MI, et al. Nanomedicine. 2014; 9(11):1591. [PubMed: 25321168]
31. Setyawati MI, et al. Chemical Society reviews. 2015
32. Tay CY, et al. Advanced Functional Materials. 2014; 24(38):5936.
33. Mitchell, DG.; Cohen, MS. MRI Principles. Philadelphia, PA: Saunders; 2004.
34. Lipinski MJ, et al. J. Am. Coll. Cardiol. 2008; 52(6):492. [PubMed: 18672171]
35. Bjørnerud A, Johansson L. NMR Biomed. 2004; 17(7):465. [PubMed: 15526351]
36. Yue-Jian C, et al. Drug Dev. Ind. Pharm. 2010; 36(10):1235. [PubMed: 20818962]
37. Smolensky ED, et al. Journal of Materials Chemistry B. 2013; 1(22):2818.
38. Barnett C, et al. Journal of Nanoparticle Research. 2012; 14(10):1. [PubMed: 22448125]
39. Zhang J, et al. Pharm. Res. 2014; 31(3):579. [PubMed: 24065589]
40. Sanjai C, et al. Carbohydrate Polymers. 2014; 104(0):231. [PubMed: 24607182]
41. Naha PC, et al. Journal of Materials Chemistry B. 2014; 2(46):8239.
42. Jin R, et al. Curr. Opin. Pharmacol. 2014; 18(0):18. [PubMed: 25173782]
43. Masoudi A, et al. Int. J. Pharm. 2012; 433(1–2):129. [PubMed: 22579990]
44. Jun, Y-w, et al. J. Am. Chem. Soc. 2005; 127(16):5732. [PubMed: 15839639]
45. Tromsdorf UI, et al. Nano Letters. 2009; 9(12):4434. [PubMed: 19799448]
46. Taboada E, et al. Langmuir. 2007; 23(8):4583. [PubMed: 17355158]
47. Caravan P, et al. Chem. Rev. 1999; 99(9):2293. [PubMed: 11749483]
48. Bates D, et al. PLoS One. 2014; 9(5):e97220. [PubMed: 24819929]
49. Barrow M, et al. Biomaterials Science. 2015; 3(4):608. [PubMed: 26222421]
50. Zhou Q, et al. International Journal of Nanomedicine. 2015; 10:1805. [PubMed: 25784806]
51. Sun X, et al. Acc. Chem. Res. 2015; 48(2):286. [PubMed: 25635467]
52. Zhou T, et al. J. Mater. Chem. 2012; 22(2):470.
53. Fang C, Zhang M. J. Control. Release. 2010; 146(1):2. [PubMed: 20493220]
54. Medarova Z, et al. Int. J Cancer. 2006; 118(11):2796. [PubMed: 16385568]
55. Rudin M, Weissleder R. Nature Reviews Drug Discovery. 2003; 2(2):123. [PubMed: 12563303]
56. Cha E-J, et al. J. Control. Release. 2011; 155(2):152. [PubMed: 21801769]
57. Veiseh O, et al. Cancer Res. 2009; 69(15):6200. [PubMed: 19638572]
58. Liu Y, Welch MJ. Bioconjug. Chem. 2012; 23(4):671. [PubMed: 22242601]
59. Devaraj NK, et al. Bioconjug. Chem. 2009; 20(2):397. [PubMed: 19138113]
60. Ardeshirpour Y, et al. Clin. Cancer Res. 2014; 20(13):3531. [PubMed: 24671949]
61. Tavaré R, et al. PLoS One. 2011; 6(5):e19662. [PubMed: 21637760]
62. Dassler K, et al. Invest. Radiol. 2012; 47(7):383. [PubMed: 22659596]

63. Schlachter EK, et al. International Journal of Nanomedicine. 2011; 6:1793. [PubMed: 21980242]
64. Barrefelt A, et al. International Journal of Nanomedicine. 2013; 8:3241. [PubMed: 24023513]
65. Basuki JS, et al. ACS Nano. 2013; 7(11):10175. [PubMed: 24131276]
66. Kaittanis C, et al. Nature Communications. 2014; 5(3384):1.
67. Hao H, et al. Journal of Materials Chemistry B. 2014; 2(45):7978.
68. Kawasaki ES, Player A. Nanomedicine: Nanotechnology, Biology and Medicine. 2005; 1(2):101.
69. Liu Y, et al. Int. J Cancer. 2007; 120(12):2527. [PubMed: 17390371]
70. Fang C, et al. ACS Applied Materials and Interfaces. 2015; 7(12):6674. [PubMed: 25751368]
71. Chen J, et al. Biomaterials. 2014; 35(4):1240. [PubMed: 24239110]
72. Schleich N, et al. J. Control. Release. 2014; 194(0):82. [PubMed: 25178270]
73. Hajikarimi Z, et al. IEEE Transactions on Nanobioscience. 2014; 13(4):403. [PubMed: 25051558]
74. Omuro A, DeAngelis LM. J. Am. Med. Assoc. 2013; 310(17):1842.
75. Thomas CE, et al. Nat Rev Genet. 2003; 4(5):346. [PubMed: 12728277]
76. Xing R, et al. Pharm. Res. 2014; 31(6):1377. [PubMed: 24065595]
77. Li D, et al. International Journal of Nanomedicine. 2014; 9:3347. [PubMed: 25045265]
78. Cheng R, et al. J. Control. Release. 2011; 152(1):2. [PubMed: 21295087]
79. Kievit FM, et al. Mol. Oncol. 2015; 9(6):1071. [PubMed: 25681012]
80. Steeves RA. Bull. N. Y. Acad. Med. 1992; 68(2):341. [PubMed: 1586869]
81. Christophi C, et al. Surg. Oncol. 1998; 7(1–2):83. [PubMed: 10421511]
82. Moroz P, et al. Int. J. Hyperthermia. 2002; 18(4):267. [PubMed: 12079583]
83. Kolosnjaj-Tabi J, et al. ACS Nano. 2014; 8(5):4268. [PubMed: 24738788]
84. Hu S-H, et al. Advanced Materials. 2012; 24(27):3627. [PubMed: 22689346]
85. Yu L, et al. Sci. Rep. 2014; 4:7216. [PubMed: 25427561]
86. O'Neal DP, et al. Cancer Lett. 2004; 209(2):171. [PubMed: 15159019]
87. Weissleder R. Nat. Biotechnol. 2001; 19(4):316. [PubMed: 11283581]
88. Kirui DK, et al. Nanotechnology. 2010; 21(10):105105. [PubMed: 20154383]
89. Larson TA, et al. Nanotechnology. 2007; 18(32):25101.
90. Lin AY, et al. Small. 2014; 10(16):3246. [PubMed: 24729414]
91. Zhou Z, et al. Biomaterials. 2014; 35(26):7470. [PubMed: 24881997]
92. Dougherty TJ, et al. J. Natl. Cancer Inst. 1998; 90(12):889. [PubMed: 9637138]
93. Moan J, Berg K. Photochem. Photobiol. 1991; 53(4):549. [PubMed: 1830395]
94. Nafiujjaman M, et al. Chemical Communications. 2015; 51(26):5687. [PubMed: 25715169]
95. Li Z, et al. Biomaterials. 2013; 34(36):9160. [PubMed: 24008045]
96. Shi J, et al. Biomaterials. 2013; 34(37):9666. [PubMed: 24034498]
97. Singh N, et al. Nano Reviews. 2010; 1 10.3402/nano.v1i0.5358.
98. Laurent S, et al. Expert Opin. Drug Deliv. 2014; 11(9):1449. [PubMed: 24870351]
99. Mahmoudi M, et al. Chem. Rev. 2012; 112(4):2323. [PubMed: 22216932]
100. Mahmoudi M, et al. J. Colloid Interface Sci. 2009; 336(2):510. [PubMed: 19476952]
101. Park K. ACS Nano. 2013; 7(9):7442. [PubMed: 24490875]
102. Venditto VJ, Szoka FC Jr. Advanced Drug Delivery Reviews. 2013; 65(1):80. [PubMed: 23036224]
103. Johannsen M, et al. International journal of hyperthermia : the official journal of European Society for Hyperthermic Oncology, North American Hyperthermia Group. 2007; 23(3):315.
104. Destouches D, et al. Cancer research. 2011; 71(9):3296. [PubMed: 21415166]
105. Maier-Hauff K, et al. Journal of neuro-oncology. 2011; 103(2):317. [PubMed: 20845061]
106. Matsumine A, et al. International journal of clinical oncology. 2011; 16(2):101. [PubMed: 21373775]
107. Choi HS, Frangioni JV. Mol. Imaging. 2010; 9(6):291. [PubMed: 21084027]

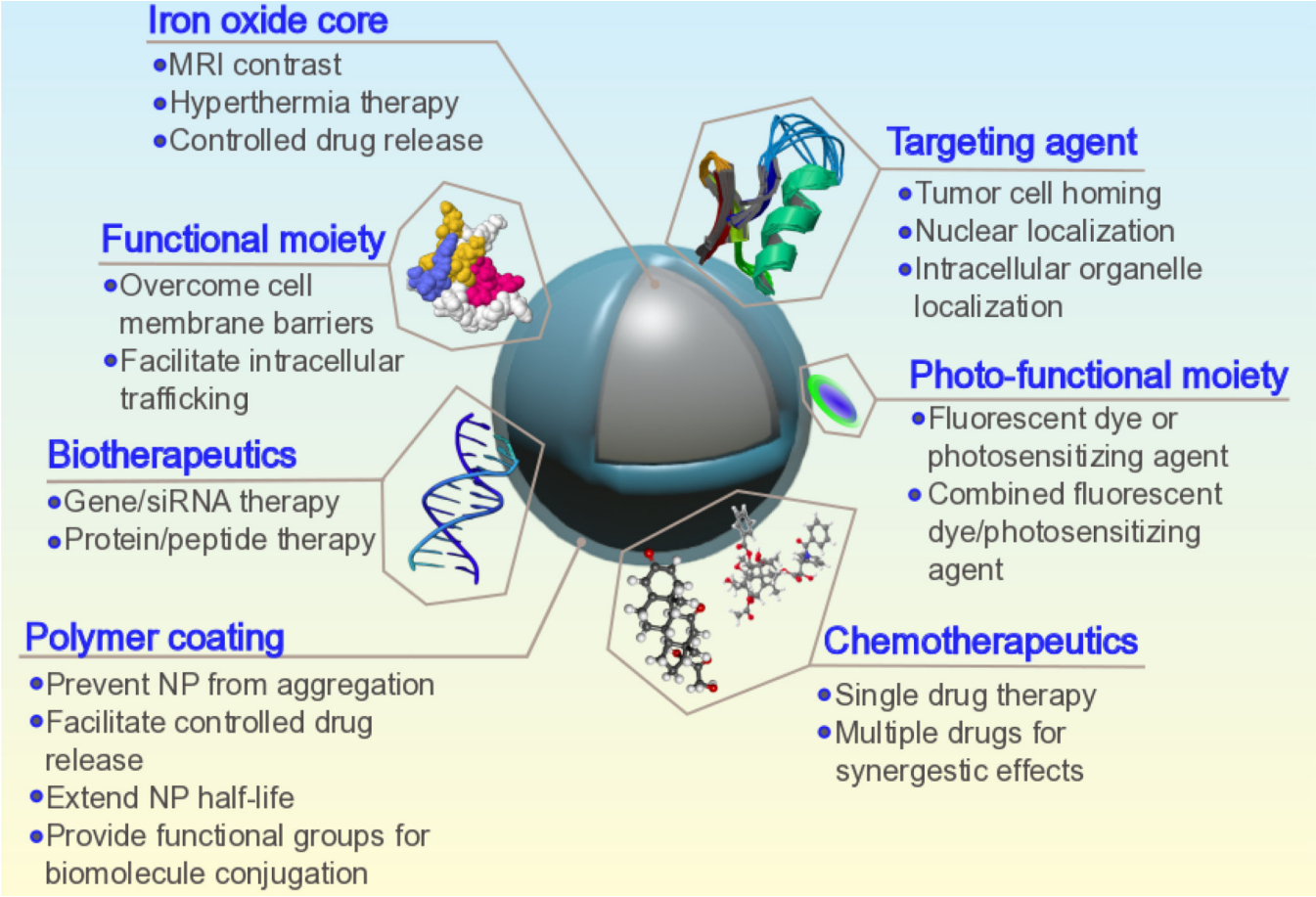

Fig.1.

Schematic illustration of a full-suite theranostic NP. The magnetite core serves as an MRI contrast agent and heat source for magnetic hyperthermia, and a polymer coating increases biocompatibility, mitigates RES uptake, and allows for facile functionalization with chemotherapeutic, biotherapeutic, optical enhancement, and targeting moieties.

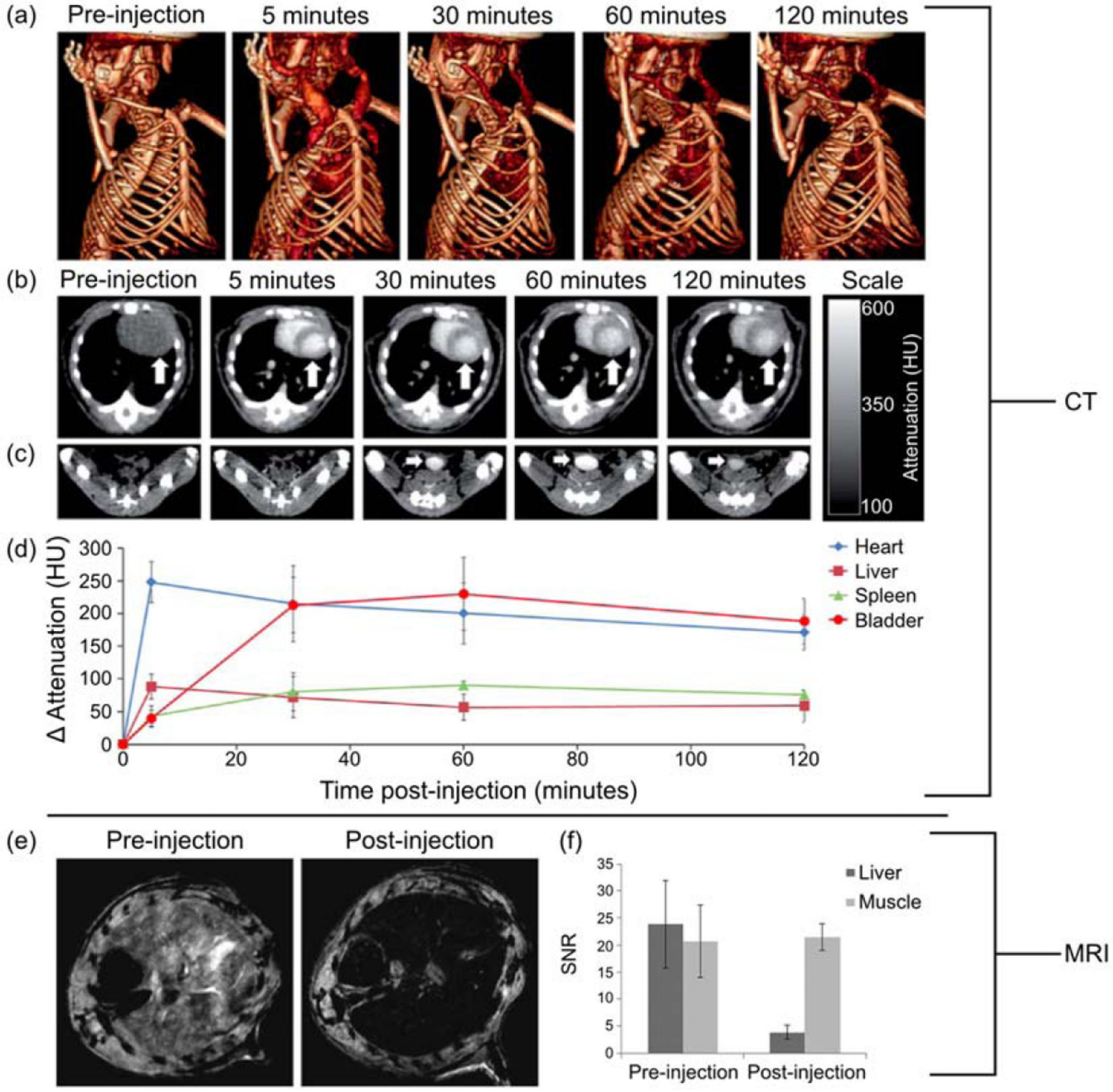

Fig. 2.

Enhanced CT and MRI contrast from dextran coated bismuth-iron oxide nanoparticles in a mouse model. (a) 3D volume rendered CT images of a mouse, pre- and 5, 30, 60, and 120 minutes post-injection. (b) CT images of a mouse thorax acquired at different time points; the arrow indicates the heart. (c) CT images of mouse groin acquired at different time points; the arrow indicates the bladder. (d) CT attenuation change of different organs over time, post-injection. (e) *In vivo* MRI of the mouse liver before and 2 hours after injection. (f) Quantitation of the MRI signal intensity in the liver compared for pre- and post-injection images. Adapted from Ref.[41] with permission of The Royal Society of Chemistry.

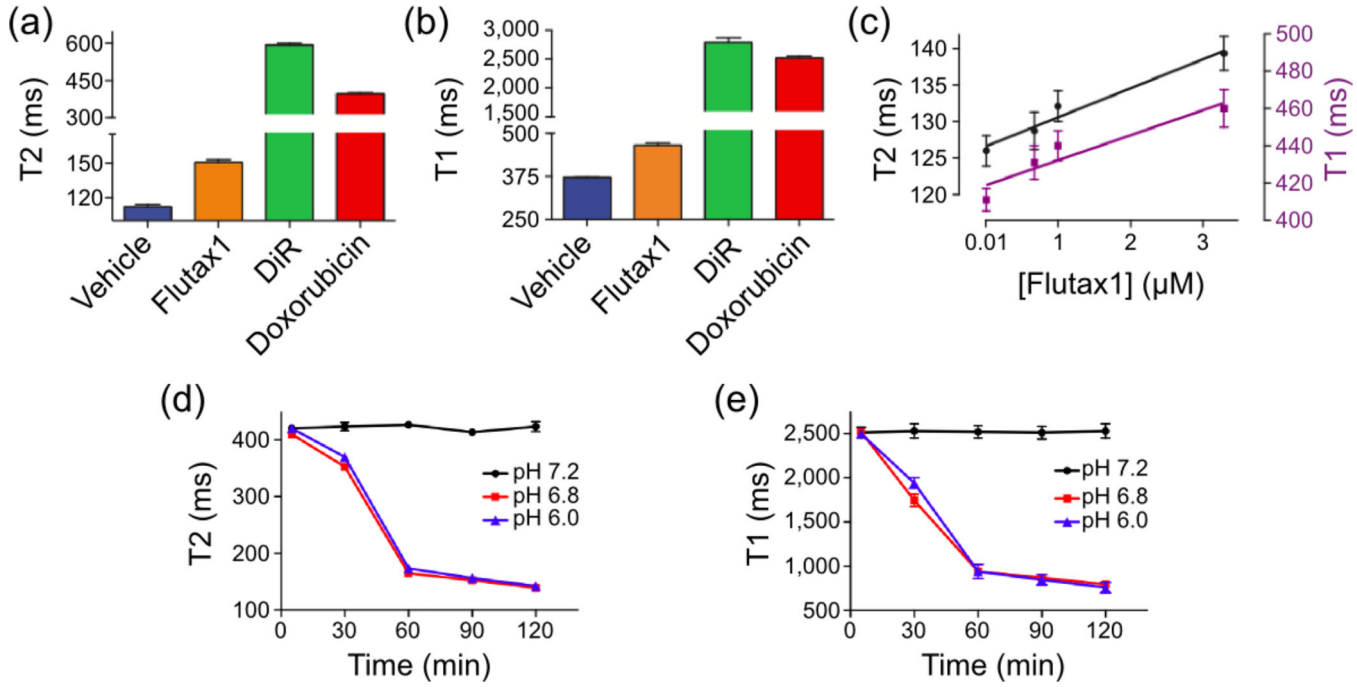

Fig. 3.

Monitoring drug delivery with SPIONs through T_1 and T_2 changes. The drugs Flutax1, DiR, and Doxorubicin increased T_2 (a) and T_1 (b) values as compared to native iron oxide (denoted as vehicle). (c) Gradual addition of Flutax1 within the iron oxide NP coating increased the formulation's T_1 and T_2 signals. As Doxorubicin was released from the NP in acidified buffers, the T_2 (d) and T_1 (e) values decreased. Adapted from Ref.[66] with permission from Nature Publishing Group.

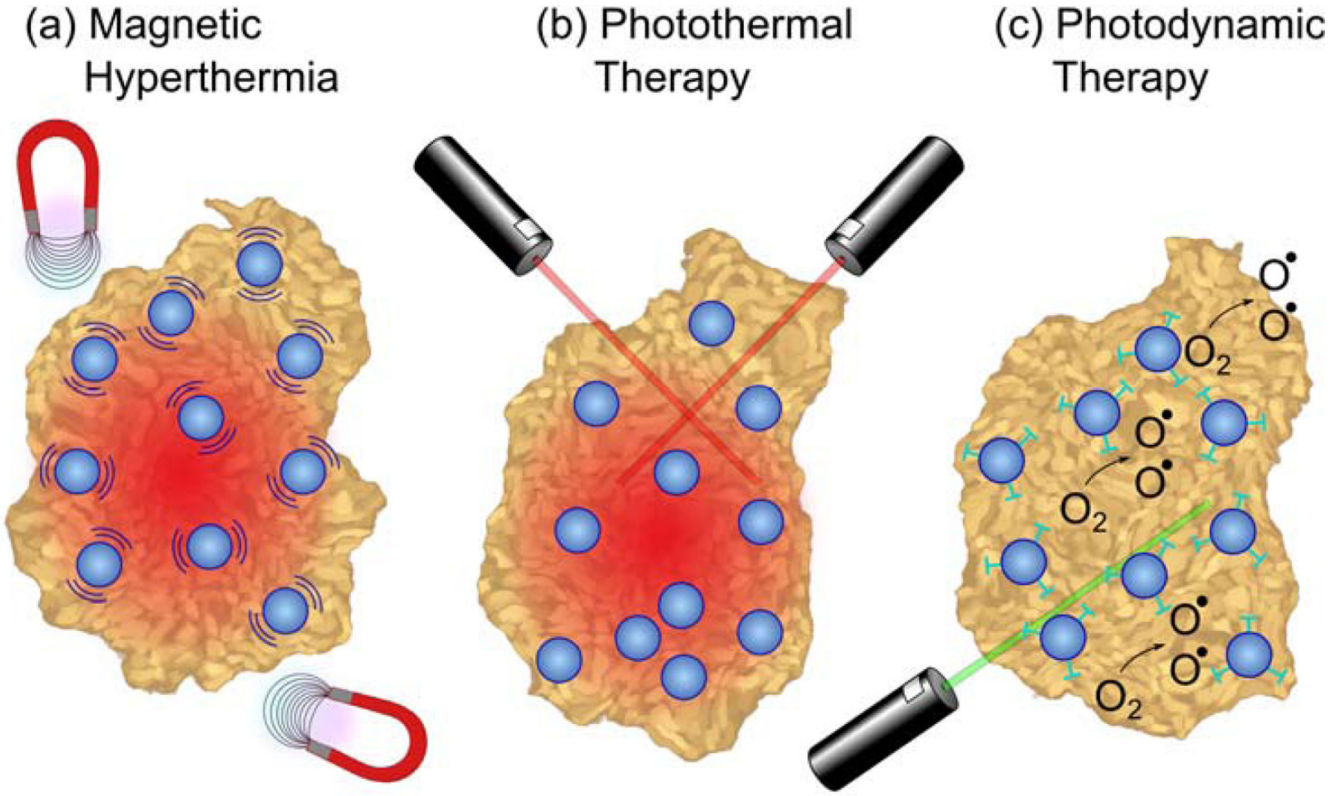

Fig. 4.

Tumor ablation therapies with iron oxide NPs. (a) In magnetic hyperthermia, an alternating magnetic field causes iron oxide NPs to generate heat, inducing tumor necrosis. (b) In photothermal ablation, light absorbed by NPs is converted to thermal energy causing cell death in the vicinity. (c) For photodynamic therapy, photosensitizing agents attached to NPs are activated by an external light source to create singlet oxygen species that are cytotoxic to cells.

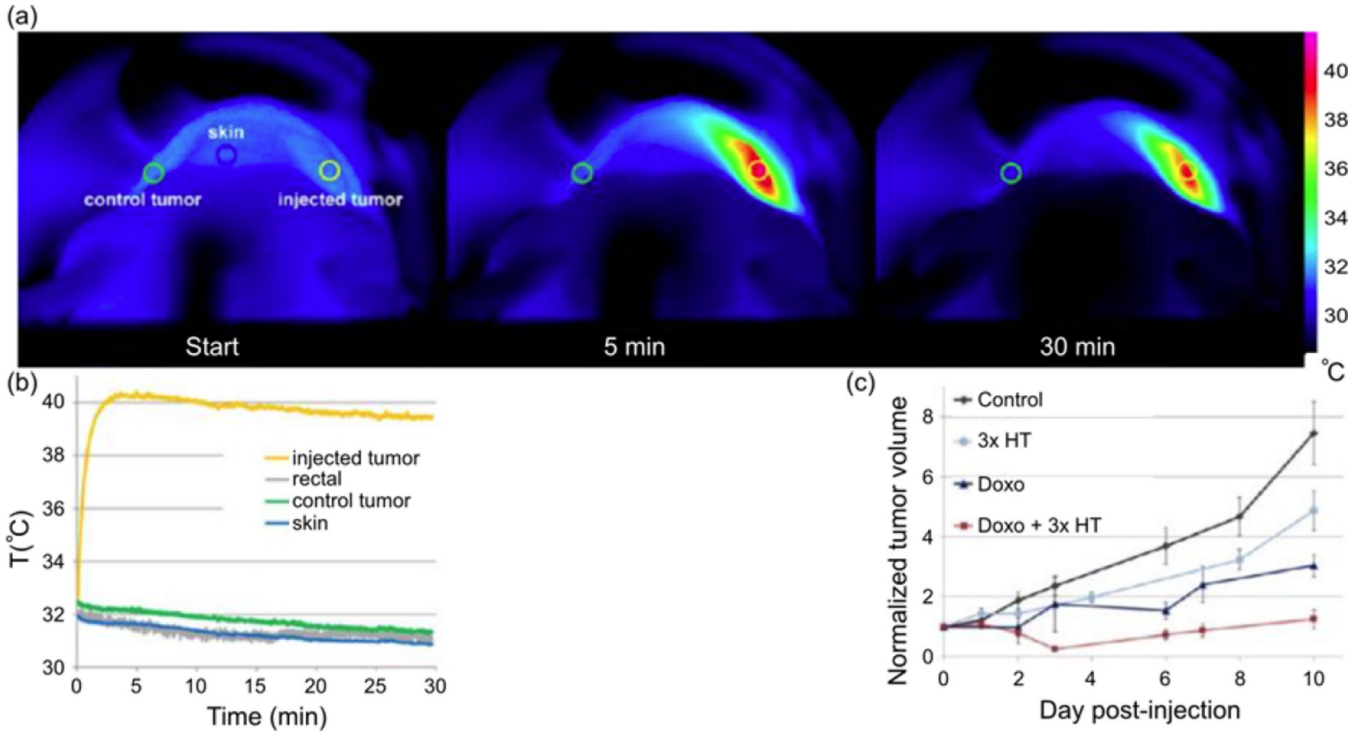

Fig. 5.

Magnetite NP-induced magnetic hyperthermia and its effect on the growth of solid tumors in mice. (a) Thermographic infrared photographs taken during exposure to an alternating magnetic field (at the starting time, 5, and 30 minutes of exposure) of a mouse intratumorally injected with iron oxide NPs. The scale bar on the right indicates the color code of the surface temperature. (b) Graph of the temperature evolution of NP-injected tumor control sites; note that only the tumor site injected with NPs (yellow) heated significantly while other tissues remained at normal temperatures. (c) Tumor growth curves of non-injected mice (Control), mice injected with NPs and exposed to an alternating magnetic field on day 0, day 1, and day 2 (3x HT), mice injected intravenously with Doxorubicin (Doxo), mice injected with Doxorubicin and NPs and exposed to an alternating magnetic field (Doxo + 3x HT). Tumor volumes are normalized to the tumor volume on day 0 when the injection was made. Adapted from Ref.[83] with permission from the American Chemical Society.

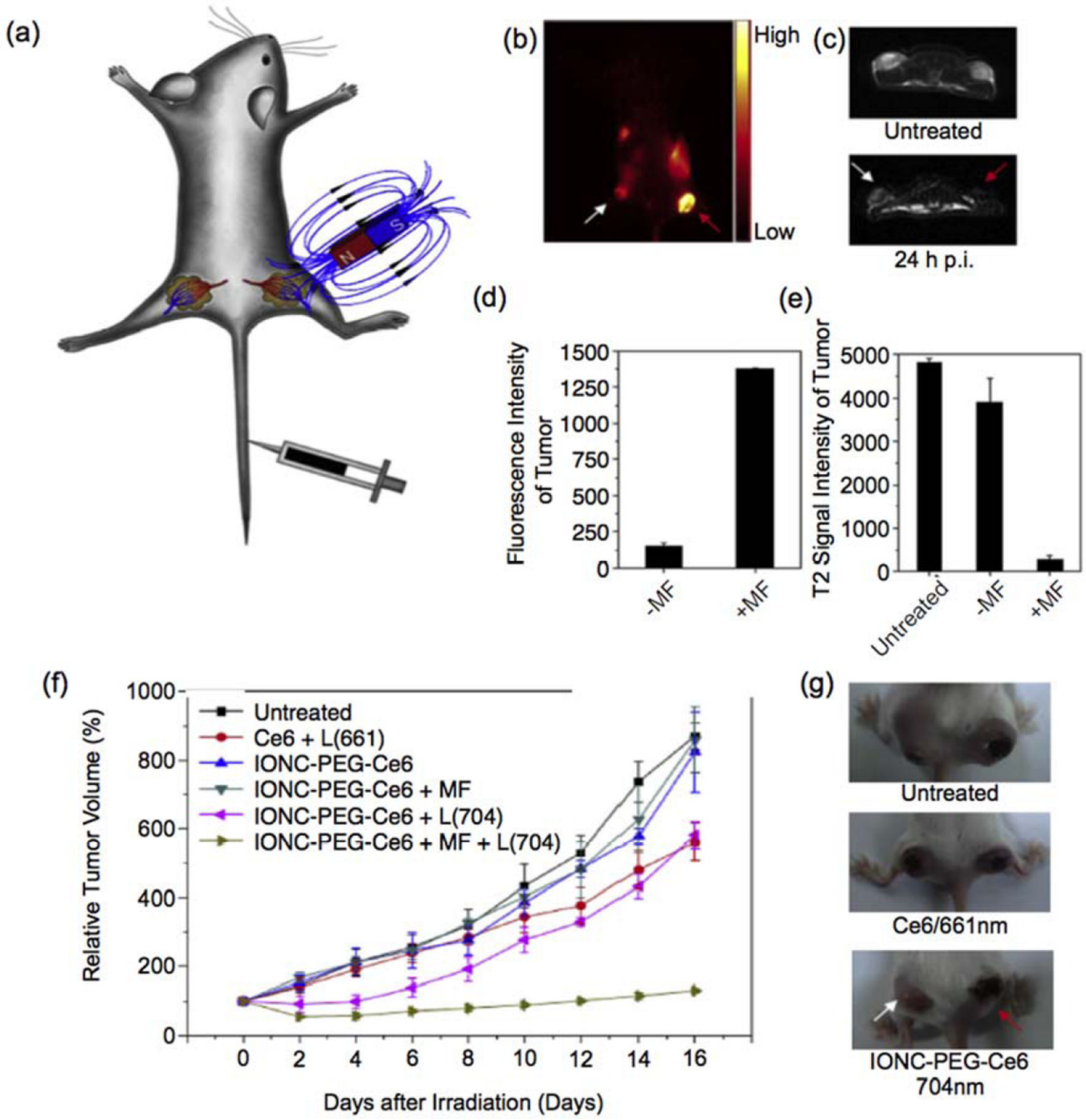

Fig. 6.

Photodynamic therapy with iron oxide nanoparticles conjugated with photosensitizing agent Ce6. (a) A schematic drawing to illustrate in vivo magnetic tumor targeting. (b) In vivo fluorescence image of a 4T1 tumor bearing mouse. (c) *In vivo* T_2-weighted MR images of a mouse taken before injection (upper) and 24 h post injection (bottom). White and red arrows point to tumors without and with a magnet attached, respectively. (d) Ce6 fluorescence signal intensities in magnetic field (MF) targeted and non-targeted tumor regions. (e) T_2-weighted MR signals of untreated, MF targeted and non-targeted tumors. (f) Tumor growth

curves of different groups of tumors after various treatments indicated. Error bars were based on SD of six tumors per group. MF: magnetic field; L: light. (g) Representative photos of mice after various treatments. White and red arrows point to tumors without and with magnetic targeting, respectively. Adapted from Ref.[95] with permission from The Royal Society of Chemistry.

Table 1

Applications of NPs in cancer imaging and therapy

NP Core Composition	NP Coating	Hydrodynamic size	Loaded Drug	Targeting Ligand	Cell/*In Vivo* Model	Application	Ref.
Bismuth-iron oxide composite	Dextran	98 nm	None	None	Human liver carcinoma cells (Hep G2) BJ5ta fibroblasts C57BL/6J mice	Dual CT and MRI T_2 contrast agents were successfully deployed in an *in vivo* murine model	41
Iron oxide	PEG	10 nm	None	None	J774 macrophages	SPIONs capable of enhancing T_1 contrast in MRI were developed and tested *in vivo*	45
Iron oxide	None	35 nm	None	Anti-prostate specific membrane antigen J591 antibody	LNCaP cells (CRL-1740) DUI145 cells (HTB-81)	MRI T_2 contrast agents that specifically target prostate cancer cells were developed	48
^{18}F-iron oxide composite	Dextran	30 nm	None	None	BALB/c mice	Trimodal imaging contrast agents providing MRI, PET, and CT capabilities were evaluated *in vivo*	59
Iron oxide	Dextran	40 nm	Flutax1 DiR Doxorubicin	None	LNCaP cells Mice with PC3 flank xenografts Mice with BT20 flank xenografts	Drug delivery vehicles that release their therapeutics in mildly acidic environments were created; these particles also exhibit changes in MR relaxivity values upon drug release and may thus be used to monitor drug delivery	66
Iron oxide	Chitosan	50 nm	Temozolomide	Chlorotoxin	Glioblastoma cells (U-118 MG) C57BL/6J mice	Drug delivery vehicles capable of carrying the chemotherapeutic temozolomide specifically to glioblastoma brain cancer cells were tested *in vitro*	70
Iron oxide	PEI	100 nm	siRNA targeting human telomerase reverse transcriptase	None	MCF-7 cells PC3 cells SKOV-3 cells Hep G2 cells BALB/c mice with Hep G2 xenograft tumors	Redox-sensitive gene and siRNA delivery was achieved *in vitro* and *in vivo* to induce apoptosis and inhibit growth of liver cancer	77
Iron oxide	Chitosan PEG PEI	40 nm	Apurinic endonuclease 1 suppressing siRNA	None	Medulloblastoma cells (UW228-1) Ependymoma cells (Res196)	*In vitro* delivery of siRNA to two types of brain tumor cells was facilitated by iron oxide NPs; the siRNA reduced the activity of an enzyme implicated in radiation resistance in tumors	79
Iron oxide	PEG	19 nm	None	None	Immunodeficient athymic NMRI mice Human epidermoid carcinoma xenografts (A431 cells)	SPIONs injected intratumorally into skin cancer xenografts induced localized hyperthermia when irradiated with an external magnetic field, arresting tumor growth	83
Iron oxide	PVA	75 – 200 nm	Doxorubicin Paclitaxel	IVO24 peptide	Human cervical carcinoma cells (HeLa) Human breast carcinoma	Dual-drug loaded, therapeutic delivery vehicles that release drugs upon exposure to an external magnetic field were used to treat breast and	84

NP Core Composition	NP Coating	Hydrodynamic size	Loaded Drug	Targeting Ligand	Cell/*In Vivo* Model	Application	Ref.
					cells (MCF-7) Mice bearing MCF-7 tumors	cervical cancer models *in vitro* and *in vivo*	
Gold-iron oxide composite	PEG	25 nm	None	A33 scFv antibody	Colorectal cancer cells (SW1222 and HT 29)	Active targeting of colorectal cancer cells and subsequent selective photothermal ablation of tumor tissue *in vivo*	88
Iron oxide	APTES	15 nm	Pheophorbide-A	None	Epithelial cancer cells (KB cells)	Simultaneous photodynamic therapy and dual-mode fluorescence/MR imaging of epithelial cancer cells *in vitro* was demonstrated	94
Iron oxide	PEG	100 nm	Chlorin e6	None	Murine breast cancer cells (4T1) BALB/c mice	*In vitro* and *in vivo* photodynamic therapy was used to treat breast cancer in a murine model; cancer tissue was specifically targeted by drawing NPs to tumor sites via an external magnetic field	95